Article

Electrochemically Deposited Amorphous Cobalt−Nickel-Doped Copper Oxide as an Efficient Electrocatalyst toward Water Oxidation Reaction

Muhammad Adeel Asghar, Abid Ali, Ali Haider,* Muhammad Zaheer, Talha Nisar, Veit Wagner, and Zareen Akhter*

Read Online

ACCESS | Metrics & More | Article Recommendations | SI Supporting Information

ABSTRACT: Production of hydrogen through water splitting is one of the green and the most practical solutions to cope with the energy crisis and greenhouse effect. However, oxygen evolution reaction (OER) being a sluggish step, the use of precious metal-based catalysts is the main impediment toward the viability of water splitting. In this work, amorphous copper oxide and doped binary- and ternary-metal oxides (containing Co^{II}, Ni^{II}, and Cu^{II}) have been prepared on the surface of fluorine-doped tin oxide by a facile electrodeposition route followed by thermal treatment. The fabricated electrodes have been employed as efficient binder-free OER electrocatalysts possessing a high electrochemical surface area due to their amorphous nature. The cobalt−nickel-doped copper oxide (ternary-metal oxide)-based electrode showed promising OER activity with a high current density of 100 mA cm^{-2} at 1.65 V versus RHE that escalates to 313 mA cm^{-2} at 1.76 V in alkaline media at pH 14. The high activity of the ternary-metal oxide-based electrode was further supported by a smaller semicircle in the Nyquist plot. Furthermore, all metal-oxide-based electrodes offered high stability when tested for continuous production of oxygen for 50 h. This work highlights the synthesis of efficient and cost-effective amorphous metal-based oxide catalysts to execute electrocatalytic OER employing an electrodeposition approach.
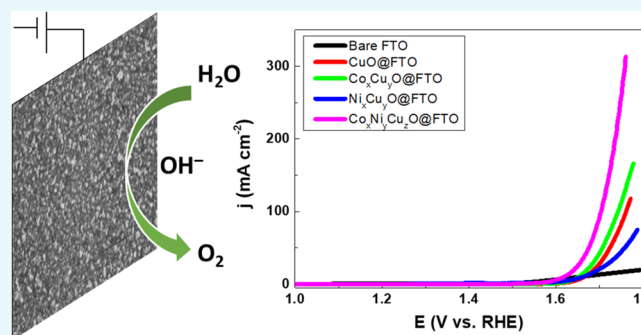
1. INTRODUCTION

The depletion and hazardous effects of fossil fuels have raised concerns to seek alternative renewable and green energy sources.[1−3] Hydrogen is a clean fuel and a charming alternate that yields water as the only byproduct during the combustion reaction. Electrocatalytic water splitting utilizes water as an abundant source to obtain hydrogen fuel and is one of the most promising and environmentally friendly routes.[4−6] However, during water electrolysis to produce hydrogen, oxygen evolution reaction (OER) at the anode is a limiting step involving a four-electron-transfer process. Due to the sluggish kinetics of the OER, a much higher potential than the thermodynamic potential is required for water oxidation that decreases the efficiency of water electrolysis.[7,8] In order to make the process more effective, efforts are being made to establish efficient electrocatalysts that minimize the required overpotential for water oxidation. State-of-the-art electrocatalysts for OER are precious-metal-based oxides of Ir, Ru, and their combinations. However, their high cost and instability during prolonged OER in basic mediums hinder their commercialization in electrochemical water splitting.[9−12] Therefore, there is a need for highly efficient, cost-effective, and stable electrocatalysts to facilitate OER reaction kinetics.

A wide range of different nanomaterials with multiple advantages over conventional materials has been used to explore their potential toward electrochemical water splitting. Nanomaterials such as carbon nanotubes, graphene, metal−organic framework, polyoxometalates, and polymers and their composites are under intensive investigation for their use in energy-related processes.[13−19] Several transition-metal-based nanomaterial electrocatalysts have been explored including metal oxides,[20−23] double-layered hydroxides,[24,25] sulfides,[12,26] selenides,[27,28] and phosphides[29−32] as favorable candidates for OER. Due to the low-cost and facile synthesis, transition-metal-based oxides are an attractive substitute for RuO_2 and IrO_2 for water oxidation. In this regard, mixed-metal oxides and doped-metal oxides have also been employed as advantageous strategies for the tuning of the electrocatalytic properties of the material.[21,33,34] In general, crystalline materials have remained

the focus of research for water splitting, whereas electrocatalytic properties of amorphous materials have rarely been explored due to their characterization difficulty. It has recently been reported that amorphous materials may outperform their crystalline counterpart with improved electrochemical activity and lower overpotential values. Better electrocatalytic properties may be ascribed to the surface defects and abundant dangling bonds that may furnish additional active sites to attain enhanced electrochemical properties.[35−38] Electrodeposition is a facile, cost-effective, and environmentally friendly method for the preparation of amorphous materials imparting high surface roughness and surface area for better electrocatalytic activity. An added advantage of electrodeposition over the various routes adopted for the synthesis of these materials is its binder-free approach with greater stickiness to the substrate and higher activity.[39,40]

In this work, we report the development of efficient and cost-effective electrocatalytic electrodes with amorphous nature and homogeneity of the catalyst deposited through a binder-free approach. We have synthesized amorphous copper oxide (CuO@FTO), cobalt-doped copper oxide (Co$_x$Cu$_y$O@FTO), nickel-doped copper oxide (Ni$_x$Cu$_y$O@FTO), and cobalt−nickel-doped copper oxide (Co$_x$Ni$_y$Cu$_z$O@FTO) through electrochemical deposition followed by the annealing method. The polarization curves, Tafel slopes, and electrochemical impedance studies of Co$_x$Ni$_y$Cu$_z$O@FTO showed superior electrocatalytic properties as compared to the other synthesized oxides. This was further supported by the higher double-layer capacitance (C_{dl}) of Co$_x$Ni$_y$Cu$_z$O@FTO and its larger electrochemical surface area (ECSA) providing more active sites for the electron-transfer process. Moreover, the smaller diameter of the semicircle in the Nyquist plot corresponds to the lesser charge-transfer resistance for Co$_x$Ni$_y$Cu$_z$O@FTO. Chronoamperometric studies reflected the stability of all fabricated electrodes when tested for the continuous production of oxygen for 50 h.

2. RESULTS AND DISCUSSION

Powder X-ray diffraction (PXRD) patterns were recorded for all prepared samples. None of the fabricated electrodes showed any obvious peaks for the deposited films, reflecting that the synthesized catalysts are predominately X-ray amorphous.[41] Figure 1 shows the XRD patterns for CuO@FTO and doped binary- and ternary-metal oxides at the fluorine-doped tin oxide (FTO) surface compared to the reference SnO$_2$ [JCPDS 00-002-1337]. It is obvious from the overlay that sharp peaks in the range of 20 to 75° 2θ values obtained for all fabricated electrodes belong to the FTO substrate.

The morphological and textural information of all fabricated electrodes was assessed by scanning electron microscopy (SEM) analysis. The images for Co$_x$Ni$_y$Cu$_z$O@FTO are shown in Figure 2, whereas that of binary-metal oxide-based electrodes are shown in Figures S1−S3. Figure 2a,b illustrates the uniform distribution of the nearly spherical particles of Co$_x$Ni$_y$Cu$_z$O@ FTO. The grain size was observed to be in the range of 40−120 nm, while the estimated average grain size was 75 nm (as given in the inset of Figure 2a). When the surface of the electrode material was examined at lower magnification, corn-like segments of the agglomerated particles were observed (see Figure 2c,d). Energy dispersive X-ray (EDX) spectra showed the presence of Co, Cu, Ni, and oxygen in the synthesized metal oxide films (S4). Elemental mapping of Cu, Ni, Co, and O, as shown in Figures 3 and S5−S7, clearly elaborated the growth of their respective oxide with a uniform distribution over the
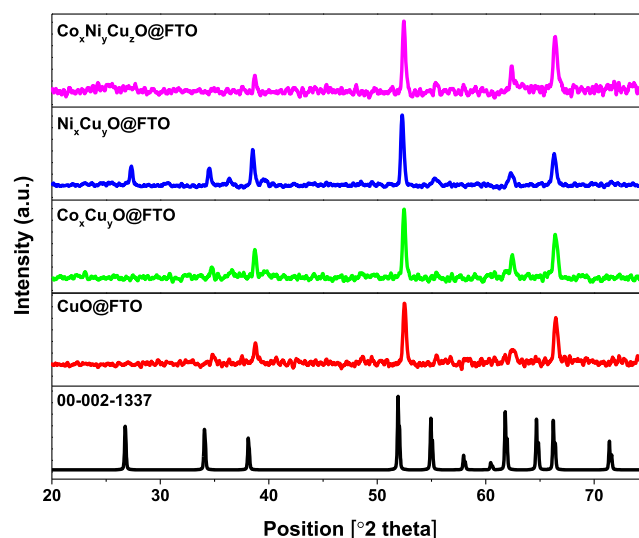

Figure 1. XRD patterns of CuO@FTO, Co$_x$Cu$_y$O@FTO, Ni$_x$Cu$_y$O@ FTO, and Co$_x$Ni$_y$Cu$_z$O@FTO compared with SnO$_2$ reference.

surface of the FTO substrate. The elemental X-ray maps for Co$_x$Ni$_y$Cu$_z$O@FTO (Figure 3) show the spatial distribution of Ni, Cu, Co, and O in the deposited film. However, mapping of Cu and O shows accumulated concentrations in some regions that indicate the agglomeration of CuO.

Further exploration of surface electronic properties and oxidation states of fabricated electrodes was carried out by XPS analysis. In Figure 4, the photoelectron spectra and the fits for Cu 2p$_{1/2}$ and 2p$_{3/2}$, Co 2p$_{1/2}$ and 2p$_{3/2}$, Ni 2p$_{1/2}$, and 2p$_{3/2}$ doublets and O 1s peaks are shown. It was found that all metals were present in a +2 oxidation state. Three peaks were observed at the binding energies of 779.6, 932.9, and 855.8 eV that were assigned to Co 2p$_{3/2}$, Cu 2p$_{3/2}$, and Ni 2p$_{3/2}$, respectively, and correspond to their respective oxides, that is, CoO, CuO, and NiO. The minor shifts in the binding energies may be ascribed to the different chemical environments.[42,43] The spectrum of the Co 2p (Figure 4a) exhibits mainly a doublet with a binding energy of 779.6 and 794.9 eV for Co 2p$_{3/2}$ and 2p$_{1/2}$, respectively, which is in the range of CoO (Co^{2+}).[44] A minor difference of 0.1 eV is attributed to the different chemical environments. Similarly, the spectrum of Ni 2p (Figure 4b) also consists of a doublet with a binding energy of 855.8 eV for 2p$_{3/2}$ which is attributed to the +2 oxidation state of Ni.[45] The spectrum of the Cu 2p consists of a doublet with a binding energy of 932.9 and 952.6 eV for the Cu 2p$_{3/2}$ and 2p$_{1/2}$, respectively, which are attributed to the +2 oxidation state of copper. In the spectrum of Cu 2p, shake-up satellite peaks are visible at higher binding energies as compared to the main photoelectron peaks with a singlet or irregular doublets which is the characteristic of copper in the +2 oxidation state.[46] The spectrum of O 1s peak exhibits four components at 529.6, 531, 531.9, and 533 eV where the peak at 529.6 eV is attributed to CoO and CuO.[44,47] The peak at 531 eV is attributed to NiO.[44] The minor peaks at 531.9 and 533 eV are attributed to the surface contaminations which could be due to the transport of the sample from the electrodeposition setup to the XPS chamber.

Electrocatalytic OER performance of binary- and ternary-metal oxide-based electrodes was examined in alkaline solution (1 M KOH) with a standard three-electrode system. The fabricated electrodes were electrochemically tested using linear
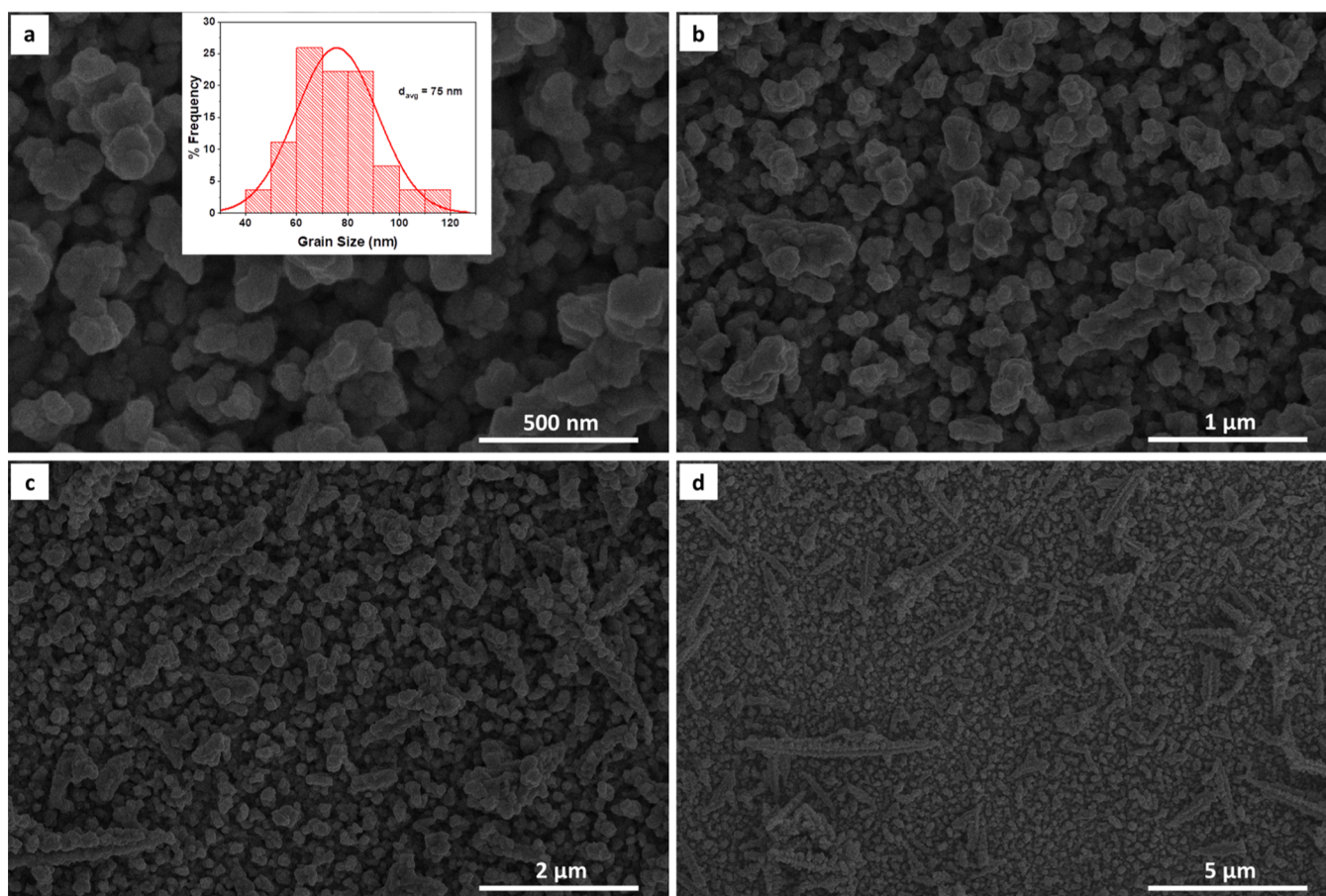
Figure 2. SEM images (a−d) of Co$_x$Ni$_y$Cu$_z$O@FTO at different magnifications. The inset (a) gives the average grain size of Co$_x$Ni$_y$Cu$_z$O@FTO.

sweep voltammetry in the range of 0 to 1.8 V versus RHE at a 5 mV/s scan rate. Figure 5a represents overlaid polarization curves of the bare FTO and modified ones with mono-, binary-, and ternary-metal oxides. Overpotential at 10 mA cm^{-2} for CuO@FTO, Ni$_x$Cu$_y$O@FTO, and Co$_x$Cu$_y$O@FTO were observed at 436, 433, and 422 mV, respectively, that increases to 530 mV for CuO@FTO and 513 mV for Co$_x$Cu$_y$O@FTO at 100 mA cm^{-2}. Compared to these, overpotential for Co$_x$Ni$_y$Cu$_z$O@FTO was significantly reduced to 388 mV at 10 mA cm^{-2} and 475 mV at 100 mA cm^{-2} which depicted its superior electrocatalytic OER performance. Electrochemical performance in terms of kinetics for OER was further investigated by the Tafel slope (Figure 5b) derived from polarization curves.

Tafel slopes calculated from the Tafel plots were found to be ∼89.7, ∼110, and ∼86 mV/dec for CuO@FTO, Ni$_x$Cu$_y$O@FTO, and Co$_x$Cu$_y$O@FTO, respectively. The lower value of the Tafel slope for Co$_x$Cu$_y$O@FTO (86.3 mV/dec) among binary-metal oxides depicts its better performance in terms of faster kinetics, while Ni$_x$Cu$_y$O@FTO has the lower performance with 110 mV/dec value of the Tafel slope. This reveals that the binary-metal combination of Cu along with Co enhanced the material performance with favorable kinetics due to more active sites in electrochemical OER. Comparative to mono- and binary-metal oxides, Co$_x$Ni$_y$Cu$_z$O@FTO has a much lower value of the Tafel slope, that is, ∼71 mV/dec indicating a much higher reaction rate for the electrochemical water splitting process in the ternary-metal oxide. This may be ascribed to more active sites and high surface area possessed by Co$_x$Ni$_y$Cu$_z$O@FTO than mono- and binary-metal oxide-based electrodes.

Cyclic voltammetry (CV) was performed in the non-faradaic region at various scan rates to assess the double-layer capacitance and ECSA of the fabricated electrodes (Figure S8). When the scan rate was plotted versus the current density, a linear relationship was observed that was then fitted using a linear function to obtain the C_{dl} for each electrode (inset of Figure S8). Electrochemical parameters such as overpotential at 10 and 100 mA cm^{-2} current densities, Tafel slope values, C_{dl}, ECSA, and roughness factor (RF) for each sample electrode are given in Table 1.

C_{dl} at the electrode−electrolyte interface is an important parameter that is correlated with the ECSA of electrode material; the higher the double-layer capacitance, the greater the ECSA.[48] In the case of binary-metal oxides, C_{dl} values for Co$_x$Cu$_y$O@FTO and Ni$_x$Cu$_y$O@FTO are 25.55 and 52.42 μF, respectively (see in Figure S8). In comparison with binary-metal oxides, Co$_x$Ni$_y$Cu$_z$O@FTO exhibited a much higher C_{dl} value, that is, 71.80 μF, which is due to the higher surface area along with more defects and consequently more active-site availability, resulting in its higher efficiency. The highest ECSA, that is, 1.772 cm^2 and RF, that is, 5.90 cm^2 was observed for Co$_x$Ni$_y$Cu$_z$O@FTO, supporting its enhanced electrochemical OER activity compared to that of binary-metal oxides. The organized array design along with its amorphous nature may also provide minimal bubble adhesion and high RF that produce extensive channels to facilitate the release of gas apart from the surface of the electrode, thus avoiding aggregation of bubbles and preventing catalysts peeling off from the substrate.[40,49]
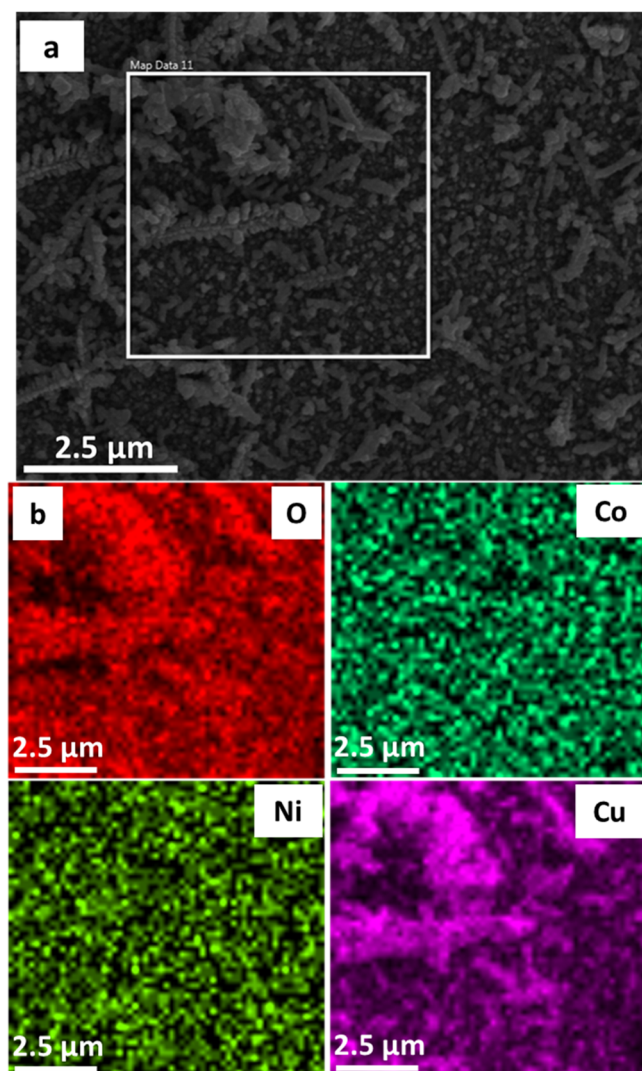
Figure 3. (a) SEM image and its (b) energy-dispersive spectra for the elemental X-ray mapping of $Co_xNi_yCu_zO$@FTO.

Electrochemical impedance spectroscopy was employed to investigate the mechanistic insights into the high OER activity of the metal oxide-based electrodes as shown in Figure 5c. The real part of impedance was plotted against its imaginary part in the Nyquist plot where the diameter of the semicircle in the high-frequency region shows the charge-transfer resistance for electrocatalysts, revealing electron-transfer kinetics at the interface of the electrode.[50] $Co_xNi_yCu_zO$@FTO exhibited a small semicircle, indicating lower charge-transfer resistance and hence a faster electron-transfer process for OER without using any binder or conductive additive. The smallest semicircle for ternary-metal oxide endorses its highest electrochemical activity compared to that of mono- and binary-metal oxides. In summary, the highest OER activity of electrodeposited $Co_xNi_yCu_zO$@FTO can be attributed to the following different factors; first, the high RF provided a larger surface area which improved the interaction of the electrolyte and the active site of the electrode, resulting in the accelerated mass transport (electrolyte diffusion) phenomenon. Second, the synergistic effect of the ternary-metal system facilitated the fast kinetics for improved OER activity.

The stability of the electrode is also a crucial criterion to evaluate the performance and durability of electrocatalysts in electrochemical water-splitting reactions.[51,52] The stability of the synthesized electrodes was tested using the chronoamperometric technique while steadily generating oxygen in 1 M KOH aqueous solution at a constant potential corresponding to 10 mA cm^{-2} for CuO@FTO, Co_xCu_yO@FTO, and Ni_xCu_yO@FTO for 50 h, while in the case of $Co_xNi_yCu_zO$@FTO, a potential corresponding to 100 mA cm^{-2} was applied. Figure 5d indicates the stability outcome for CuO@FTO and its binary-metal oxides, and the inset shows the response of $Co_xNi_yCu_zO$@FTO. All metal oxide electrocatalysts showed good stability in the amperometric measurements. Admirable electrocatalytic stability was observed for $Co_xNi_yCu_zO$@FTO that displayed the robust behavior of ternary-metal catalyst toward OER at a current density of 100 mA cm^{-2} representing a good candidate for the electrocatalytic water oxidation reaction. The stability of $Co_xNi_yCu_zO$@FTO was also explored by cycling the electrode continuously for 5000 cycles at a scan rate of 5 mV/s and comparing the polarization curves before and after cycling as shown in Figure 6. The polarization curve obtained after running 5000 cyclic voltammetric scans was similar to that obtained before the cycles, validating the high stability of the electrode in an alkaline medium.

3. CONCLUSIONS

In summary, we have adopted a binder-free approach to synthesize CuO@FTO and its doped binary- and ternary-metal oxide electrodes of Cu, Co, and Ni via the electrodeposition method followed by thermal treatment. Electrochemical studies for CuO@FTO and doped metals oxides have been carried out for the electrode performance in the electrochemical water oxidation reaction. Amorphous structures of these fabricated electrodes expose the greater area of the catalysts that lead to enhanced ECSA and RF. The amorphous structures of electrode materials also have a crucial impact on avoiding bubbling over the surface of the electrode, which is another advantage over the electrodes developed by drop-casting. It is evident that the ternary-metal oxide exhibits admirable OER activity with an overpotential of 388 mV to attain 10 mA cm^{-2}. Greater ECSA and higher RF of the fabricated amorphous $Co_xNi_yCu_zO$@FTO electrode substantially boosted its electrocatalytic activity toward OER in water splitting. Other electrochemical parameters such as Tafel slope, double-layer capacitance, and charge-transfer resistance also showed improved results, which may be ascribed to the synergic effect and greater number of active sites resulting from roughness. Facile synthesis, binder-free electrode fabrication, higher electrochemical activity, and better long-term stability, that is, for 50 h at 100 mA cm^{-2} render $Co_xNi_yCu_zO$@FTO as a potential candidate for scale-up application in electrochemical water oxidation. By considering the remarkable performance and low-cost materials required for the fabrication of the electrode, the synthesized electrocatalysts show broad prospects for future energy demands.

4. EXPERIMENTAL SECTION

The water used in all experiments was purified through a deionizer system. Nickel(II) sulfate hexahydrate, copper(II) sulfate hexahydrate, and cobalt(II) chloride hexahydrate were acquired from Sigma-Aldrich; boric acid, potassium hydroxide, and sulfuric acid were purchased from Alfa Aesar; while acetone, isopropyl alcohol, and FTO-coated glass (TEC 15, Hartford Glass Co., 15 Ω/sq, $50 \times 13 \times 2.3$ mm^3) were purchased commercially. All chemicals were used as received.
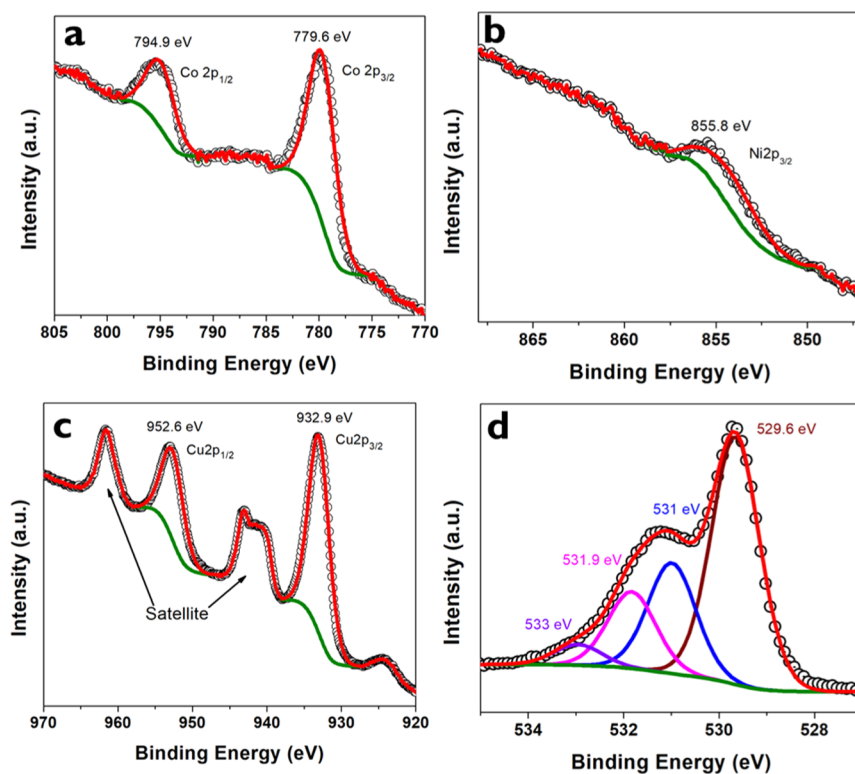
Figure 4. XPS core-level spectra of (a) Co 2p, (b) Ni 2p, (c) Cu 2p, and (d) O 1s for $Co_xCu_yNi_zO$@FTO.
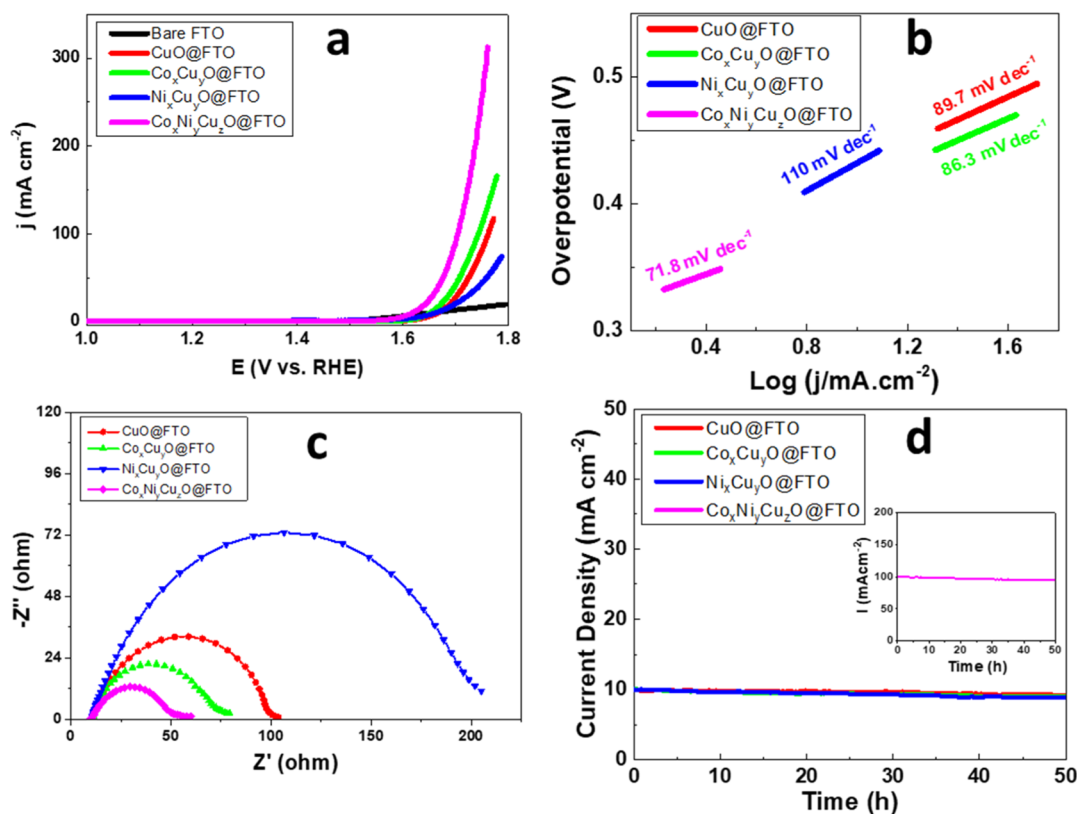

Figure 5. (a) *iR* corrected polarization curves at a scan rate of 5 mV/s, (b) Tafel plot, (c) electrochemical impedance spectroscopic measurements, and (d) chronoamperometric analysis for the stability of CuO@FTO, Ni_xCu_yO@FTO, and Co_xCu_yO@FTO at a potential corresponding to 10 mA cm^{-2}. The inset shows the stability of $Co_xNi_yCu_zO$@FTO at a potential corresponding to 100 mA cm^{-2}.

Doped binary- and ternary-metal oxide-based electrodes were prepared by electrochemical deposition using a Gamry Interface

1010e galvanostat/potentiostat followed by the annealing procedure. From a larger FTO-coated sheet, 1 cm long and 1

Table 1. Electrochemical Parameters for Undoped CuO and Doped Metal Oxide Electrodes[a]

catalysts	η_{10} (mV)	η_{100} (mV)	Tafel slope (mV/dec)	C_{dl} (μF)	ECSA (cm^2)	RF
CuO@FTO	436	530	89.7	18.70	0.468	1.56
Co$_x$Cu$_y$O@FTO	422	513	86.3	25.55	0.638	2.13
Ni$_x$Cu$_y$O@FTO	433		110.0	52.42	1.280	4.27
Co$_x$Ni$_y$Cu$_z$O@FTO	388	475	71.8	70.88	1.772	5.90

[a]Where η_{10} and η_{100} are overpotentials at 10 and 100 mA cm^{-2}, respectively.

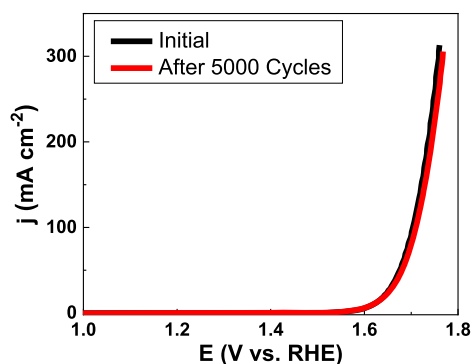**Figure 6.** *iR* corrected polarization curves for Co$_x$Ni$_y$Cu$_z$O@FTO at a scan rate of 5 mV/s before and after 5000 CV cycles.

cm wide section was cut, and an area of 0.3 cm^2 was exposed to the deposition bath masking the rest area by a Teflon tape. The substrate was rinsed thoroughly with deionized water and then sonicated in detergent, deionized water, acetone, and isopropyl alcohol for 15 min each followed by drying in air flux. Electrochemical deposition of metals on FTO-coated glass was performed using the galvanostatic method. The electro-deposition was carried out in a three-electrode cell containing an equimolar electrolytic solution of respective metal salts in the presence of 8 mM boric acid. The pH of the prepared solution was adjusted to 3 using H$_2$SO$_4$. Galvanostatic electrodeposition was performed at −10 mA cm^{-2} for 300 s using FTO-coated glass as a working electrode, Ag/AgCl as a reference electrode, and Pt wire as a counter electrode. The deposited samples were then washed with an excess of deionized water to remove any unreacted species and dried overnight. Oxidation of the samples to their respective oxides was carried out by annealing in air at 350 °C for 2 h.

Scanning electron micrographs were obtained by using FEI Nova SEM 230 coupled with a Bruker EDX system at an accelerating voltage of 3 kV. PXRD analyses were carried out on a PANalytical X'Pert multipurpose X-ray diffraction system having a Cu anode with a Kα radiation source, using a scan range of 2θ = 10−80°. For XPS, the sample was mounted onto a holder with a conducting carbon-tape to avoid surface charging during the measurements. The sample was introduced to the ultra-high-vacuum vessel which contains a photoelectron spectrometer having a hemispherical analyzer (Specs Phoibos 100) and Mg/Al X-ray gun (Specs XR-50) with a 45° angle. In this experiment, Mg Kα radiation with an energy of 1253.6 eV was used as an excitation source. The pass energy was kept at 50 eV. The pressure in the chamber was approx. 1 × 10^{-9} mbar. The measured data were fitted using CasaXPS software, and the background was subtracted using Shirley's method. A simplified Voigt function was used for fitting with the sample full width at half maximum (FWHM) for doublet, and the ratio between 2p$_{3/2}$ and 2p$_{1/2}$ was 0.5.

Electrochemical experiments were performed in a conventional three-electrode cell in 1 M KOH using the Gamry Interface 1010e galvanostat/potentiostat. The fabricated working electrodes were of 1 × 1 cm^2 dimension, while platinum wire and saturated Ag/AgCl were used as the counter electrode and the reference electrode, respectively. All measured potential values were converted to RHE using the formula $E_{RHE} = E_{Ag/AgCl}$ + 0.197 + 0.059 × pH, where pH of the solution used was 14. Tafel plots were obtained by plotting overpotential (η) versus log(j) and the linear fragments of the Tafel plots were fitted to the Tafel equation [$\eta = b \log(j) + a$, where b is Tafel slope, j is current density, and a is exchange current density].[19] Electrochemical impedance was measured in the frequency range of 100 kHz to 0.1 Hz with a small AC signal of 10 mV. All potential values were *iR* compensated and current densities reported were obtained by dividing the current by the geometric surface area of the respective electrodes.

ASSOCIATED CONTENT

ⓢ Supporting Information

The Supporting Information is available free of charge at https://pubs.acs.org/doi/10.1021/acsomega.1c01251.

SEM images, EDX spectra, elemental mapping, and CV measurements (PDF)

AUTHOR INFORMATION

Corresponding Authors

Ali Haider − *Department of Chemistry, Quaid-i-Azam University, Islamabad 45320, Pakistan; Pakistan Academy of Science, Islamabad 44000, Pakistan;* ⓘ orcid.org/0000-0001-8755-2454; Phone: +92 51 90642130; Email: ahaider@qau.edu.pk; Fax: +92 51 90642241

Zareen Akhter − *Department of Chemistry, Quaid-i-Azam University, Islamabad 45320, Pakistan;* ⓘ orcid.org/0000-0002-5010-0291; Phone: +92 51 90642111; Email: zareen_a@qau.edu.pk, zareenakhter@yahoo.com; Fax: +92 51 90642241

Authors

Muhammad Adeel Asghar − *Department of Chemistry, Quaid-i-Azam University, Islamabad 45320, Pakistan*

Abid Ali − *Department of Chemistry, The University of Lahore, Lahore 54000, Pakistan;* ⓘ orcid.org/0000-0002-0452-4827

Muhammad Zaheer − *Department of Chemistry and Chemical Engineering, Syed Babar Ali School of Science and Engineering, Lahore University of Management Sciences (LUMS), Lahore 54792, Pakistan;* ⓘ orcid.org/0000-0003-2389-4396

Talha Nisar − *Physics and Earth Sciences, Jacobs University Bremen, Bremen 28759, Germany*

Veit Wagner − *Physics and Earth Sciences, Jacobs University Bremen, Bremen 28759, Germany;* ⓘ orcid.org/0000-0002-6831-8600

■ REFERENCES

(1) Chu, S.; Cui, Y.; Liu, N. The path towards sustainable energy. *Nat. Mater.* **2017**, *16*, 16−22.

(2) Faber, M. S.; Jin, S. Earth-abundant inorganic electrocatalysts and their nanostructures for energy conversion applications. *Energy Environ. Sci.* **2014**, *7*, 3519−3542.

(3) Lewis, N. S.; Nocera, D. G. Powering the planet: Chemical challenges in solar energy utilization. *Proc. Natl. Acad. Sci. U.S.A.* **2006**, *103*, 15729−15735.

(4) Mao, S. S.; Shen, S.; Guo, L. Nanomaterials for renewable hydrogen production, storage and utilization. *Prog. Nat. Sci.: Mater. Int.* **2012**, *22*, 522−534.

(5) Li, X.; Hao, X.; Abudula, A.; Guan, G. Nanostructured catalysts for electrochemical water splitting: current state and prospects. *J. Mater. Chem. A* **2016**, *4*, 11973−12000.

(6) Wang, J.; Yue, X.; Yang, Y.; Sirisomboonchai, S.; Wang, P.; Ma, X.; Abudula, A.; Guan, G. Earth-abundant transition-metal-based bifunctional catalysts for overall electrochemical water splitting: A review. *J. Alloys Compd.* **2020**, *819*, 153346.

(7) Lyons, M. E. G.; Doyle, R. L.; Fernandez, D.; Godwin, I. J.; Browne, M. P.; Rovetta, A. The mechanism and kinetics of electrochemical water oxidation at oxidized metal and metal oxide electrodes. Part 1. General considerations: A mini review. *Electrochem. Commun.* **2014**, *45*, 60−62.

(8) Diaz-Morales, O.; Calle-Vallejo, F.; de Munck, C.; Koper, M. T. M. Electrochemical water splitting by gold: evidence for an oxide decomposition mechanism. *Chem. Sci.* **2013**, *4*, 2334−2343.

(9) Mamaca, N.; Mayousse, E.; Arrii-Clacens, S.; Napporn, T. W.; Servat, K.; Guillet, N.; Kokoh, K. B. Electrochemical activity of ruthenium and iridium based catalysts for oxygen evolution reaction. *Appl. Catal., B* **2012**, *111−112*, 376−380.

(10) Stoerzinger, K. A.; Qiao, L.; Biegalski, M. D.; Shao-Horn, Y. Orientation-Dependent Oxygen Evolution Activities of Rutile IrO_2 and RuO_2. *J. Phys. Chem. Lett.* **2014**, *5*, 1636−1641.

(11) Shi, Q.; Zhu, C.; Du, D.; Lin, Y. Robust noble metal-based electrocatalysts for oxygen evolution reaction. *Chem. Soc. Rev.* **2019**, *48*, 3181−3192.

(12) Anantharaj, S.; Ede, S. R.; Sakthikumar, K.; Karthick, K.; Mishra, S.; Kundu, S. Recent Trends and Perspectives in Electrochemical Water Splitting with an Emphasis on Sulfide, Selenide, and Phosphide Catalysts of Fe, Co, and Ni: A Review. *ACS Catal.* **2016**, *6*, 8069−8097.

(13) Biegun, M.; Chen, X.; Mijowska, E. Cobalt/Carbon Nanocomposite as Oxygen Evolution Reaction Electrocatalyst. *ChemElectroChem* **2018**, *5*, 2681−2685.

(14) Li, R. J.; Qi, Y. F.; Wang, Q.; Wang, J. J.; Liu, Z. Y.; Wang, X. G.; Zhao, X. J.; Yang, E. C. Heterometallic Feed Ratio-Dominated Oxygen Evolution Activity in Self-Supported Metal-Organic Framework Nanosheet Arrays Electrocatalyst. *Z. Anorg. Allg. Chem.* **2020**, *646*, 1412−1418.

(15) Lee, C.; Jeon, D.; Park, J.; Lee, W.; Park, J.; Kang, S. J.; Kim, Y.; Ryu, J. Tetraruthenium Polyoxometalate as an Atom-Efficient Bifunctional Oxygen Evolution Reaction/Oxygen Reduction Reaction Catalyst and Its Application in Seawater Batteries. *ACS Appl. Mater. Interfaces* **2020**, *12*, 32689−32697.

(16) Haider, A.; Bassil, B. S.; Soriano-López, J.; Qasim, H. M.; Sáenz de Pipaón, C.; Ibrahim, M.; Dutta, D.; Koo, Y.-S.; Carbó, J. J.; Poblet, J. M.; Galán-Mascarós, J. R.; Kortz, U. 9-Cobalt(II)-Containing 27-Tungsto-3-germanate(IV): Synthesis, Structure, Computational Modeling, and Heterogeneous Water Oxidation Catalysis. *Inorg. Chem.* **2019**, *58*, 11308−11316.

(17) Bhunia, S.; Bhunia, K.; Patra, B. C.; Das, S. K.; Pradhan, D.; Bhaumik, A.; Pradhan, A.; Bhattacharya, S. Efficacious Electrochemical Oxygen Evolution from a Novel Co(II) Porphyrin/Pyrene-Based Conjugated Microporous Polymer. *ACS Appl. Mater. Interfaces* **2019**, *11*, 1520−1528.

(18) He, W.; Bai, X.; Ma, J.; Wang, S.; Zhang, B.; Shao, L.; Chen, H.; Li, L.; Fu, Y.; Chen, J. Fabrication of hierarchically flower-like trimetallic coordination polymers via ion-exchange strategy for efficient electrocatalytic oxygen evolution. *J. Electroanal. Chem.* **2021**, *883*, 115036.

(19) Ping, J.; Wang, Y.; Lu, Q.; Chen, B.; Chen, J.; Huang, Y.; Ma, Q.; Tan, C.; Yang, J.; Cao, X.; Wang, Z.; Wu, J.; Ying, Y.; Zhang, H. Self-assembly of single-layer CoAl-layered double hydroxide nanosheets on 3D graphene network used as highly efficient electrocatalyst for oxygen evolution reaction. *Adv. Mater.* **2016**, *28*, 7640−7645.

(20) Song, F.; Bai, L.; Moysiadou, A.; Lee, S.; Hu, C.; Liardet, L.; Hu, X. Transition Metal Oxides as Electrocatalysts for the Oxygen Evolution Reaction in Alkaline Solutions: An Application-Inspired Renaissance. *J. Am. Chem. Soc.* **2018**, *140*, 7748−7759.

(21) Kim, J. S.; Kim, B.; Kim, H.; Kang, K. Recent Progress on Multimetal Oxide Catalysts for the Oxygen Evolution Reaction. *Adv. Energy Mater.* **2018**, *8*, 1702774.

(22) Jiang, R.; Baker, D. R.; Tran, D. T.; Li, J.; Leff, A. C.; Zhang, S. S. Multimetallic $FeCoNiO_x$ Nanoparticles Covered with Nitrogen-Doped Graphene Layers as Trifunctional Catalysts for Hydrogen Evolution and Oxygen Reduction and Evolution. *ACS Appl. Nano Mater.* **2020**, *3*, 7119−7129.

(23) Inamdar, A. I.; Chavan, H. S.; Pawar, S. M.; Kim, H.; Im, H. NiFeCo oxide as an efficient and sustainable catalyst for the oxygen evolution reaction. *Int. J. Energy Res.* **2020**, *44*, 1789−1797.

(24) Yang, L.; Liu, Z.; Zhu, S.; Feng, L.; Xing, W. Ni-based layered double hydroxide catalysts for oxygen evolution reaction. *Mater. Today Phys.* **2021**, *16*, 100292.

(25) Rohit, R. C.; Jagadale, A. D.; Shinde, S. K.; Kim, D.-Y.; Kumbhar, V. S.; Nakayama, M. Hierarchical nanosheets of ternary CoNiFe layered double hydroxide for supercapacitors and oxygen evolution reaction. *J. Alloys Compd.* **2021**, *863*, 158081.

(26) Chauhan, M.; Deka, S. Hollow Cobalt Sulfide Nanoparticles: A Robust and Low-Cost pH-Universal Oxygen Evolution Electrocatalyst. *ACS Appl. Energy Mater.* **2020**, *3*, 977−986.

(27) Masud, J.; Liyanage, W. P. R.; Cao, X.; Saxena, A.; Nath, M. Copper Selenides as High-Efficiency Electrocatalysts for Oxygen Evolution Reaction. *ACS Appl. Energy Mater.* **2018**, *1*, 4075−4083.

(28) Wang, Z.; Li, J.; Tian, X.; Wang, X.; Yu, Y.; Owusu, K. A.; He, L.; Mai, L. Porous Nickel−Iron Selenide Nanosheets as Highly Efficient Electrocatalysts for Oxygen Evolution Reaction. *ACS Appl. Mater. Interfaces* **2016**, *8*, 19386−19392.

(29) Li, J.; Yan, M.; Zhou, X.; Huang, Z.-Q.; Xia, Z.; Chang, C.-R.; Ma, Y.; Qu, Y. Mechanistic Insights on Ternary $Ni_{2−x}Co_xP$ for Hydrogen Evolution and Their Hybrids with Graphene as Highly Efficient and Robust Catalysts for Overall Water Splitting. *Adv. Funct. Mater.* **2016**, *26*, 6785−6796.

(30) Tan, Y.; Wang, H.; Liu, P.; Shen, Y.; Cheng, C.; Hirata, A.; Fujita, T.; Tang, Z.; Chen, M. Versatile nanoporous bimetallic phosphides towards electrochemical water splitting. *Energy Environ. Sci.* **2016**, *9*, 2257−2261.

(31) Du, C.; Yang, L.; Yang, F.; Cheng, G.; Luo, W. Nest-like NiCoP for Highly Efficient Overall Water Splitting. *ACS Catal.* **2017**, *7*, 4131−4137.

(32) Yuan, G.; Bai, J.; Zhang, L.; Chen, X.; Ren, L. The effect of P vacancies on the activity of cobalt phosphide nanorods as oxygen evolution electrocatalyst in alkali. *Appl. Catal., B* **2021**, *284*, 119693.

(33) Truong, L.; Roy, S. B.; Jerng, S.-K.; Jeon, J. H.; Lee, S.; Chun, S.-H. Facile electrodeposition of V-doped CoP on vertical graphene for efficient alkaline water electrolysis. *RSC Adv.* **2020**, *10*, 13016−13020.

(34) Chen, C.; Tuo, Y.; Lu, Q.; Lu, H.; Zhang, S.; Zhou, Y.; Zhang, J.; Liu, Z.; Kang, Z.; Feng, X.; Chen, D. Hierarchical trimetallic Co-Ni-Fe oxides derived from core-shell structured metal-organic frameworks for highly efficient oxygen evolution reaction. *Appl. Catal., B* **2021**, *287*, 119953.

(35) Li, L.; Shao, Q.; Huang, X. Amorphous Oxide Nanostructures for Advanced Electrocatalysis. *Chem.—Eur. J.* **2020**, *26*, 3943−3960.

(36) Li, L.; Wang, P.; Shao, Q.; Huang, X. Metallic nanostructures with low dimensionality for electrochemical water splitting. *Chem. Soc. Rev.* **2020**, *49*, 3072−3106.

(37) Balram, A.; Zhang, H.; Santhanagopalan, S. Enhanced Oxygen Evolution Reaction Electrocatalysis via Electrodeposited Amorphous α-Phase Nickel-Cobalt Hydroxide Nanodendrite Forests. *ACS Appl. Mater. Interfaces* **2017**, *9*, 28355−28365.

(38) Liang, H.; Gandi, A. N.; Xia, C.; Hedhili, M. N.; Anjum, D. H.; Schwingenschlögl, U.; Alshareef, H. N. Amorphous NiFe-OH/NiFeP Electrocatalyst Fabricated at Low Temperature for Water Oxidation Applications. *ACS Energy Lett.* **2017**, *2*, 1035−1042.

(39) Han, S.; Liu, S.; Wang, R.; Liu, X.; Bai, L.; He, Z. One-Step Electrodeposition of Nanocrystalline $Zn_xCo_{3-x}O_4$ Films with High Activity and Stability for Electrocatalytic Oxygen Evolution. *ACS Appl. Mater. Interfaces* **2017**, *9*, 17186−17194.

(40) Barati Darband, G.; Aliofkhazraei, M.; Hyun, S.; Shanmugam, S. Pulse Electrodeposition of a Superhydrophilic and Binder-Free Ni−Fe−P Nanostructure as Highly Active and Durable Electrocatalyst for Both Hydrogen and Oxygen Evolution Reactions. *ACS Appl. Mater. Interfaces* **2020**, *12*, 53719−53730.

(41) Irshad, A.; Munichandraiah, N. Electrodeposited Nickel-Cobalt-Sulfide Catalyst for the Hydrogen Evolution Reaction. *ACS Appl. Mater. Interfaces* **2017**, *9*, 19746−19755.

(42) Wang, A.-L.; Xu, H.; Li, G.-R. NiCoFe layered triple hydroxides with porous structures as high-performance electrocatalysts for overall water splitting. *ACS Energy Lett.* **2016**, *1*, 445−453.

(43) Villarroel-Rocha, J.; Barrera, D.; Sapag, K. Introducing a self-consistent test and the corresponding modification in the Barrett, Joyner and Halenda method for pore-size determination. *Microporous Mesoporous Mater.* **2014**, *200*, 68−78.

(44) McIntyre, N. S.; Cook, M. G. X-ray photoelectron studies on some oxides and hydroxides of cobalt, nickel, and copper. *Anal. Chem.* **1975**, *47*, 2208−2213.

(45) Dufresne, P.; Payen, E.; Grimblot, J.; Bonnelle, J. P. Study of nickel-molybdenum-.gamma.-aluminum oxide catalysts by x-ray photo-electron and Raman spectroscopy. Comparison with cobalt-molybde-num-.gamma.-aluminum oxide catalysts. *J. Phys. Chem.* **1981**, *85*, 2344−2351.

(46) Khawaja, E. E.; Salim, M. A.; Khan, M. A.; Al-Adel, F. F.; Khattak, G. D.; Hussain, Z. XPS, auger, electrical and optical studies of vanadium phosphate glasses doped with nickel oxide. *J. Non-Cryst. Solids* **1989**, *110*, 33−43.

(47) McIntyre, N. S.; Sunder, S.; Shoesmith, D. W.; Stanchell, F. W. Chemical information from XPS—applications to the analysis of electrode surfaces. *J. Vac. Sci. Technol.* **1981**, *18*, 714−721.

(48) Anjum, M. A. R.; Lee, J. S. Sulfur and Nitrogen Dual-Doped Molybdenum Phosphide Nanocrystallites as an Active and Stable Hydrogen Evolution Reaction Electrocatalyst in Acidic and Alkaline Media. *ACS Catal.* **2017**, *7*, 3030−3038.

(49) Li, Y.; Zhang, H.; Xu, T.; Lu, Z.; Wu, X.; Wan, P.; Sun, X.; Jiang, L. Under-water superaerophobic pine-shaped Pt nanoarray electrode for ultrahigh-performance hydrogen evolution. *Adv. Funct. Mater.* **2015**, *25*, 1737−1744.

(50) Ren, X.; Ji, X.; Wei, Y.; Wu, D.; Zhang, Y.; Ma, M.; Liu, Z.; Asiri, A. M.; Wei, Q.; Sun, X. In situ electrochemical development of copper oxide nanocatalysts within a TCNQ nanowire array: a highly conductive electrocatalyst for the oxygen evolution reaction. *Chem. Commun.* **2018**, *54*, 1425−1428.

(51) Geng, J.; Kuai, L.; Kan, E.; Wang, Q.; Geng, B. Precious-Metal-Free Co−Fe−O/rGO Synergetic Electrocatalysts for Oxygen Evolution Reaction by a Facile Hydrothermal Route. *ChemSusChem* **2015**, *8*, 659−664.

(52) Guo, X.; Feng, Z.; Lv, Z.; Bu, Y.; Liu, Q.; Zhao, L.; Hao, C.; Li, G.; Lei, Q. Formation of Uniform FeP Hollow Microspheres Assembled by Nanosheets for Efficient Hydrogen Evolution Reaction. *ChemElectroChem* **2017**, *4*, 2052−2058.